

# Giant electrophononic response in $\text{PbTiO}_3$ by strain engineering

Pol Torres,<sup>1</sup> Jorge Íñiguez,<sup>2,3</sup> and Riccardo Rurali<sup>1</sup>

<sup>1</sup>*Institut de Ciència de Materials de Barcelona (ICMAB-CSIC)*

*Campus de Bellaterra, 08193 Bellaterra, Barcelona, Spain*

<sup>2</sup>*Materials Research and Technology Department,*

*Luxembourg Institute of Science and Technology (LIST),*

*Avenue des Hauts-Fourneaux 5, L-4362 Esch/Alzette, Luxembourg*

<sup>3</sup>*Physics and Materials Science Research Unit,*

*University of Luxembourg, 41 Rue du Brill, L-4422 Belvaux, Luxembourg*

(Dated: November 5, 2019)

## Abstract

We demonstrate theoretically how, by imposing epitaxial strain in a ferroelectric perovskite, it is possible to achieve a dynamical control of phonon propagation by means of external electric fields, which yields a giant electrophononic response, i.e. the dependence of the lattice thermal conductivity on external electric fields. Specifically, we study the strain-induced manipulation of the lattice structure and analyze its interplay with the electrophononic response. We show that tensile biaxial strain can drive the system to a regime where the electrical polarization can be effortlessly rotated and thus yield giant electrophononic responses that are at least one order of magnitude larger than in the unstrained system. These results derive directly from the almost divergent behavior of the electrical susceptibility at those critical strains that drive the polarization on the verge of a spontaneous rotation.

PACS numbers:

Heat in insulators and semiconductors is carried by phonons, the quanta of lattice vibrations, and the thermal conductivity is determined by the associated dissipative processes. The manipulation of phonons and the dynamical tuning of the thermal conductivity of a solid are problems of fundamental interest in condensed matter physics [1–3] and have important implications in renewable energy applications –such as vibrational energy harvesting [4], thermoelectricity [5] or electrocaloric cooling [6]– and for the implementation of a phonon-based logic, which relies on thermal diodes [7, 8] and transistors [9], and where information is transmitted and processed by heat carriers.

Ferroelectric materials favor a spontaneous lattice distortion, below a critical temperature, which has an associated dipole moment that can be controlled with an external electric field. Therefore, they are the ideal playground to explore phonon manipulation, because the modifications of the lattice structure translate directly into changes of the vibrational properties and thus of the thermal conductivity. The polarization,  $\mathbf{P}$ , can be selectively oriented, for instance, creating neighboring regions separated by domain walls, which may act as phonon scatterers or filters [10, 11]. More generally, an electric field can *strengthen* or *weaken*  $\mathbf{P}$ , when it is parallel to it, or partially rotate it, when it has a component perpendicular to it [12–14]. This *electrophononic* effect, whereby an electric field is used to tune the thermal conductivity via a controlled modification of the crystal lattice, paves the way toward an all-electrical control of the heat flux.

The temperature- and field-dependent thermal conductivity,  $\boldsymbol{\kappa}$ , can be written as a second-order expansion in terms of the thermal-response tensors  $\boldsymbol{\alpha}$  and  $\boldsymbol{\beta}$  as

$$\kappa_{ij}(T, \mathbf{E}) = \kappa_{ij}^0(T) + \sum_k \alpha_{ij,k}(T) E_k + \sum_{kl} \beta_{ij,kl}(T) E_k E_l , \quad (1)$$

where  $i$ ,  $j$ ,  $k$ , and  $l$  are the spatial directions  $x$ ,  $y$ , and  $z$  and  $\boldsymbol{\kappa}^0$  is the conductivity at zero applied field. The physical mechanisms that lead to a coupling between  $\mathbf{E}$  and  $\boldsymbol{\kappa}$  are different for fields parallel or perpendicular to  $\mathbf{P}$ . As shown in Ref. 12 by some of us, in the former case the applied field results in a hardening of the phonon frequencies throughout the whole spectrum, if  $\mathbf{E}$  is parallel to  $\mathbf{P}$ , or a softening, if it is anti-parallel to it. In the latter case the main effect of the applied field is lowering the symmetry of the lattice, thus leading

to a larger phase-space for phonon-phonon anharmonic scattering processes [12, 13]. The reported changes in the thermal conductivity are large, but typically require applied electric fields that are substantial. In this Letter we study the dependence of the electrophononic coefficients  $\alpha$  and  $\beta$  on epitaxial strain and show that suitable strain conditions can increase them by one order of magnitude and result, in principle, in nearly divergent responses at certain critical strains, where a vanishing small electric field leads to large variation of the thermal conductivity.

We focus on  $\text{PbTiO}_3$  (PTO), a paradigmatic ferroelectric oxide with a tetragonal perovskite structure and a critical temperature of 760 K, and consider biaxial tensile strains,  $\epsilon$ , in the plane perpendicular to the tetragonal axis of the ground state up to 3%. Note that biaxial strains within this range can be routinely achieved by epitaxially growing PTO thin films on appropriate substrates [15]; further, the strain can also be controlled dynamically if a piezoelectric substrate is used [16, 17].

We calculate the ground-state structure, the harmonic and third-order anharmonic force constants (IFCs) within second-principles density-functional theory (SPDFT). The term second-principles refer to methods that are first-principles-based both in their formulation and in the way the information needed to use them is obtained [18]. We use the implementation of the SCALE-UP code [18, 19], which relies on polynomial potentials fitted from DFT calculations. As most first-principles approaches, SPDFT reproduces accurately the vibrational and response properties of PTO [19] and it has a documented predictive power for the most important structural, vibrational and response properties of ferroelectric perovskite oxides [20, 21]. We compute the IFCs in supercells defined as an  $8 \times 8 \times 8$  repetition of the 5-atom unit cell using the finite differences method. For the harmonic displacements we use the PHONOPY code [22] considering all neighboring interactions. THIRDDORDER.PY [23, 24] is used to determine the anharmonic interactions, neglecting those beyond twelfth neighbors, a choice that we checked yields converged results. The IFCs calculated within the SPDFT framework are used to obtain an iterative solution of linearized phonon Boltzmann Transport Equation (BTE) [25] with the SHENGBTE code [24], thus avoiding the shortcomings of the relaxation time approximation (RTA) that treat Normal processes as resistive scattering

events [25, 26]. The thermal conductivity is then expressed as:

$$\kappa_{ij} = \frac{1}{k_b T^2 N \Omega} \sum_{\lambda} n_{\lambda} (n_{\lambda} + 1) (\hbar \omega_{\lambda})^2 v_{i,\lambda} \tau_{\lambda} (v_{j,\lambda} + \Delta_{j,\lambda}) , \quad (2)$$

where  $N$  is the number of  $\mathbf{q}$ -points used in the sampling of the Brillouin zone,  $\Omega$  the volume of the 5-atom perovskite unit cell. The sum runs over all phonon modes, the index  $\lambda$  including both  $\mathbf{q}$ -point and phonon band.  $n_{\lambda}$  is the Bose-Einstein distribution function, and  $\omega_{\lambda}$ ,  $\tau_{\lambda}$  and  $v_{i,\lambda}$  correspond to the phonon frequency, relaxation time and group velocity,  $\partial \omega_{\lambda} / \partial q_i$ , respectively. The term  $\Delta_{j,\lambda}$  takes into account the deviation of the heat current with respect to the RTA approach and is thus relevant on those systems where Normal processes play an important role. We solve Eq. (2) on a  $8 \times 8 \times 8$   $\mathbf{q}$ -point grid and obtain the thermal conductivity,  $\kappa(T)$ , by summing over all the modes. We also include isotopic disorder scattering, using the natural abundances of isotopes of Pb, Ti, and O, within the model of Tamura [27].

We first investigate the dependence of the polarization on the applied strain, i.e. at increasing values of the substrate lattice parameter  $a_{sub}$ . As it can be seen in Fig. 1, at a critical strain of  $\epsilon^{c,1} \sim 1.25\%$  the polarization  $\mathbf{P}$ , which was initially oriented along the  $z$ -axis,  $P_z \vec{k}$ , starts rotating and for a strain of  $\epsilon^{c,2} \sim 1.73\%$  it lies entirely within the  $xy$ -plane,  $\mathbf{P} = P_x \vec{i} + P_y \vec{j}$ , with  $P_x = P_y$ . This behavior has been previously reported in PTO and in other perovskite oxides and derives from the preferential alignment of  $\mathbf{P}$  with the longer axis [28–30]. Notice that the tetragonal phase with space group  $P4mm(99)$  is only present when  $P_x = P_y = 0$  and  $P_z \neq 0$ . When  $P_x = P_y \neq 0$  and  $P_z \neq 0$ , between  $\epsilon^{c,1}$  and  $\epsilon^{c,2}$ , we find a monoclinic phase  $Cm(8)$ , and when  $\mathbf{P}$  falls into the  $xy$ -plane the structure has the orthorhombic symmetry  $Amm2(38)$ . The applied biaxial tensile strain enlarge the cell in  $xy$ -plane and shrinks it along the  $z$ -axis (equivalent to the tetragonal axis in the present case for  $\epsilon = 0$ ), tending to make the three lattice vectors similar and thus triggering the rotation of the polarization (Fig. 1, top panel). Although the reliability of the results obtained within the SPDFT approach here employed has been demonstrated in different contexts [13, 20, 21], we have explicitly verified that the  $\mathbf{P}(\epsilon)$  curves of Fig. 1 reproduce well results obtained within DFT, using the VASP code [31] with the local density approximation (LDA) and a

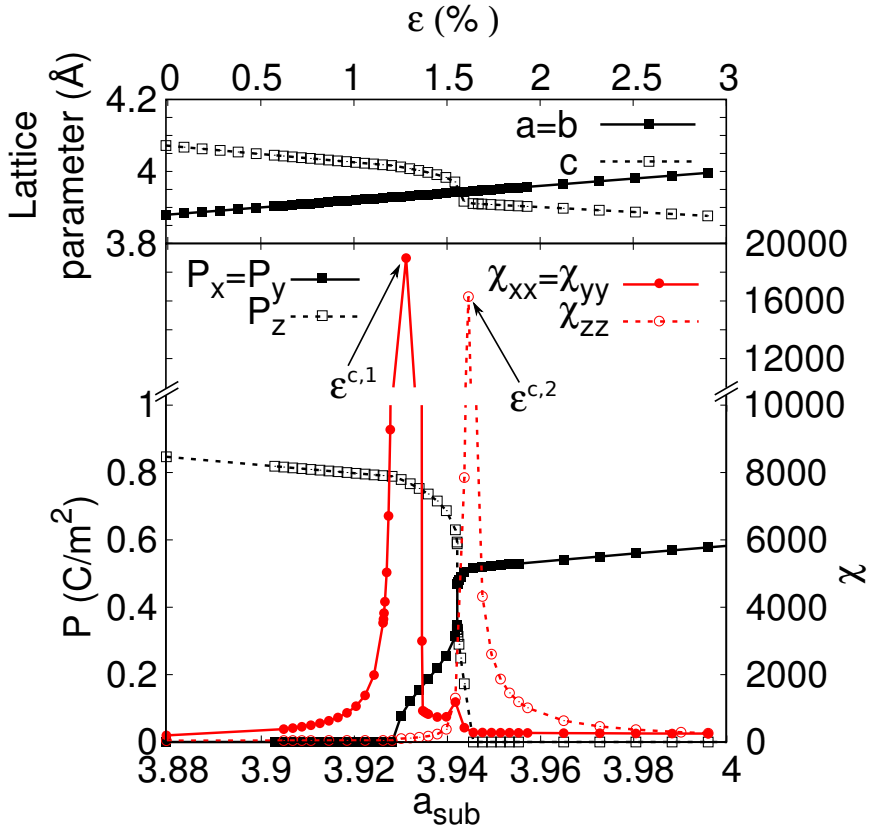


FIG. 1: (Top panel) Lattice parameters and (main panel) components of the polarization,  $\mathbf{P}$  and diagonal terms of the electrical susceptibility tensor,  $\chi$ , as a function of the substrate lattice parameter  $a_{sub}$ . The applied strain referred to the lattice parameter of the zero Kelvin cubic phase is shown in the axis above the top panel.

plane wave cutoff of 500 eV with the projector augmented-wave method [32, 33]. Note also that, in this work, we are assuming that PTO is in a mono-domain state. In reality, multi-domain configurations may form, yielding a richer behavior, and experimentally measured values of the thermal conductivity are smaller than those estimated here [34]. Nevertheless, the intrinsic properties of the domains with rotating polarization should be well captured by our calculations.

The diagonal components of the electrical susceptibility tensor,  $\chi$ , are also plotted in Fig. 1. When the strain-enabled rotation of the polarization is about to occur the sus-

ceptibility experiences an enormous increase. This behavior is an indication that in those conditions a vanishing small electric field is sufficient to induce a large change in the polarization and the attendant large structural deformation. So, for instance,  $\chi_{xx}$ , starts increasing slowly as  $a_{sub}$  grows, but when  $\epsilon$  reaches the critical value of  $\epsilon^{c,1} \sim 1.25\%$  it essentially diverges, a behavior that corresponds to the strain-driven onset of  $P_x = P_y$  in a second-order transition.  $\chi_{zz}$  has a similar behavior when  $\epsilon$  is decreased in a highly strained sample and reaches  $\epsilon^{c,2} \sim 1.73\%$ . In this case we observe a discontinuity in the polarization, with the susceptibility reaching very large values as well. This behavior is typical of weakly first-order transformations, which are common in ferroelectric perovskites like  $\text{PbTiO}_3$  [35] or  $\text{BaTiO}_3$  [36].

The effortless rotation of the polarization close to some critical strain values, reflected in the large increase of the susceptibility, hints at a similar behavior of the electrophononic coefficients. Therefore, for each of the strain values considered we have solved the phonon BTE and computed the thermal conductivity,  $\kappa$ , first without field and then applying increasingly large field values along the  $x$ - and  $z$ -axes to compute the  $\alpha$  and  $\beta$  tensors. All the results discussed from now on are calculated at 300 K and before the saturation of the dielectric response.

In absence of field, as one can observe in Fig. 2, the thermal conductivity tensor is anisotropic, as expected in a tetragonal or orthorhombic lattice. More precisely, when no strain is applied the component parallel to  $\mathbf{P}$  ( $\kappa_{zz} = 12 \text{ Wm}^{-1}\text{K}^{-1}$ ) is relatively low and almost three times smaller than the components perpendicular to  $\mathbf{P}$  ( $\kappa_{xx} = \kappa_{yy} = 30 \text{ Wm}^{-1}\text{K}^{-1}$ ). Both  $\kappa_{xx}$  and  $\kappa_{zz}$  undergo a similar decrease until the strain-enabled rotation of the polarization takes place. After that  $\kappa_{zz} > \kappa_{xx}$ , because now  $\mathbf{P}$  lies in the  $xy$ -plane, and both components remain roughly constant, with no significant dependence on strain. The anisotropy of  $\kappa$  is recovered after the full rotation of  $\mathbf{P}$  and the ratio between the independent components of  $\kappa$  is still around 2.5, though now  $\kappa_{ii}$  settle to lower values. The strain-induced change in the thermal conductivity makes  $\kappa_{xx}$  and  $\kappa_{zz}$  reach a minimum value ( $4.8$  and  $3.8 \text{ Wm}^{-1}\text{K}^{-1}$ , respectively) for  $\epsilon^{c,1} < \epsilon < \epsilon^{c,2}$ , when the material is in a monoclinic phase with both in-plane and out-of-plane polarization components. Notice that

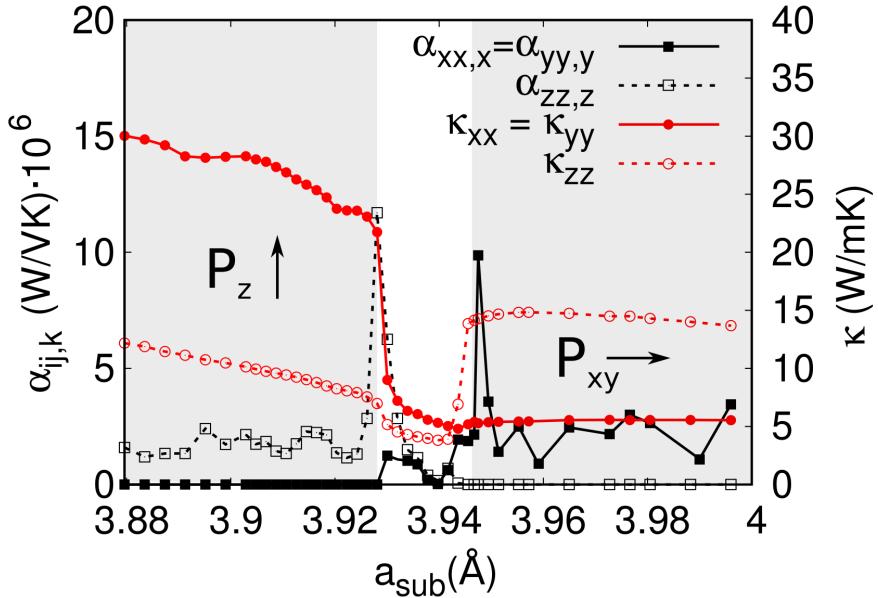


FIG. 2: Thermal conductivity and first-order electrophononic coefficient,  $\alpha_{ii,i}$ , as a function of the substrate lattice parameter  $a_{sub}$ . The polarization direction is represented to indicate when  $\mathbf{E}$  is perpendicular or in the plane of  $\mathbf{P}$ . The fluctuation of  $\alpha$  far from the critical points is caused by the error associated to the polynomial fitting of Eq. (1).

by simply applying a biaxial strain to the lattice it is possible to achieve a huge reduction of  $\kappa$ . Indeed, close to  $\epsilon^{c,1}$  and  $\epsilon^{c,2}$ ,  $\kappa_{xx}$  can be reduced a 85 % and  $\kappa_{zz}$  a 70 % compared to their values in the unstrained system.

To study electrophononic effects we have considered fields from  $5 \times 10^4$  to  $2.6 \times 10^5$  V/cm for strain values far from  $\epsilon^{c,1}$  and  $\epsilon^{c,2}$ , and smaller values of around  $10^2$  V/cm, where the response of  $\kappa$  is much stronger (see Fig. 3). The change in  $\kappa$  as a function of the electric field  $\mathbf{E}$  represented in Fig. 3 can be fitted to Eq. (1) in order to obtain the coefficients  $\alpha_{ij,k}(T)$  and  $\beta_{ij,kl}(T)$  that allow describing the electrophononic response. By using Eq. (1) we first focus on the linear electrophononic response that relates  $\kappa_{ii}$  to an electric field  $E_i$ , i.e.  $\alpha_{xx,x} = \alpha_{yy,y}$  and  $\alpha_{zz,z}$ . Our results are shown in Fig. 2. As it can be seen there,  $\alpha_{ii,i}$  has a sizeable value whenever  $\mathbf{E}$  is parallel to  $\mathbf{P}$ , i.e.  $\alpha_{zz,z}$  for  $\epsilon < 1\%$ , where  $\mathbf{P} = P_z \vec{k}$ , and  $\alpha_{xx,x} = \alpha_{yy,y}$  for  $\epsilon > 2\%$ , where  $\mathbf{P} = P_x \vec{i} + P_y \vec{j}$ . This observation agrees well with previous

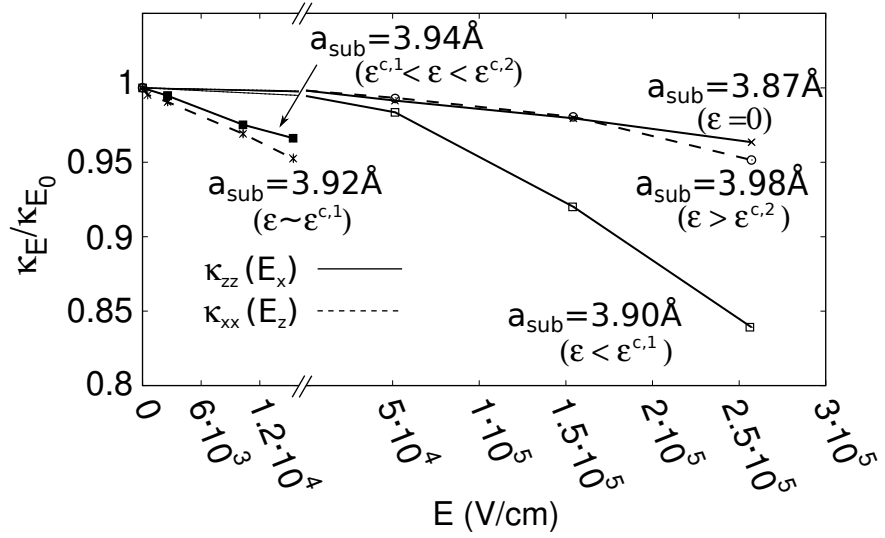


FIG. 3: Relative change of the thermal conductivity as a function of an applied electric field for different values of the biaxial strain. Solid lines show the response in  $\kappa_{zz}$  when a electric field perpendicular to the  $z$ -axis is applied. Dashed lines show the electrophononic response in  $\kappa_{xx}$  when the electric field is applied parallel to the  $z$ -axis.

reports of a dominant linear electrophononic response for fields parallel to the tetragonal axis in PTO [12]. Yet, when it approaches the critical strain values of  $\epsilon^{c,1}$  and  $\epsilon^{c,2}$ , where  $\mathbf{P}$  spontaneously rotates,  $\alpha_{ii,i}$  experiences a sudden and large increase. We found an increment of one order of magnitude, though this gain can in principle be increased by getting closer to the critical strains.

When the applied electric field is perpendicular to the polar axis, the electrophononic response of  $\kappa$  is quadratic, i.e.  $\beta \neq 0$ , while the linear term  $\alpha$  is zero by symmetry [12]. This can be observed in Fig. 2 in  $\alpha_{xx,x} = \alpha_{yy,y}$  for  $\epsilon < \epsilon^{c,1}$ , where  $\mathbf{P} = P_z \vec{k}$ , or analogously in  $\alpha_{zz,z}$  for  $\epsilon > \epsilon^{c,2}$  when  $\mathbf{P} = P_x \vec{i} + P_y \vec{j}$ . In Fig. 4 the crossed terms of the linear response  $\alpha_{ii,j}$  and  $\beta_{ii,jj}$  for  $i = j$  and  $i \neq j$  are represented. From Fig. 2 and Fig. 4 we can see that when the applied electric field is perpendicular to the polarization it always results in a quadratic reduction of the thermal conductivity, with negative electrophononic coefficients  $\beta$ , being  $\alpha = 0$ . On the contrary, when the applied electric field is parallel to the polarization  $\alpha$  is always positive. All the non-zero coefficients tend to become very large close to the critical

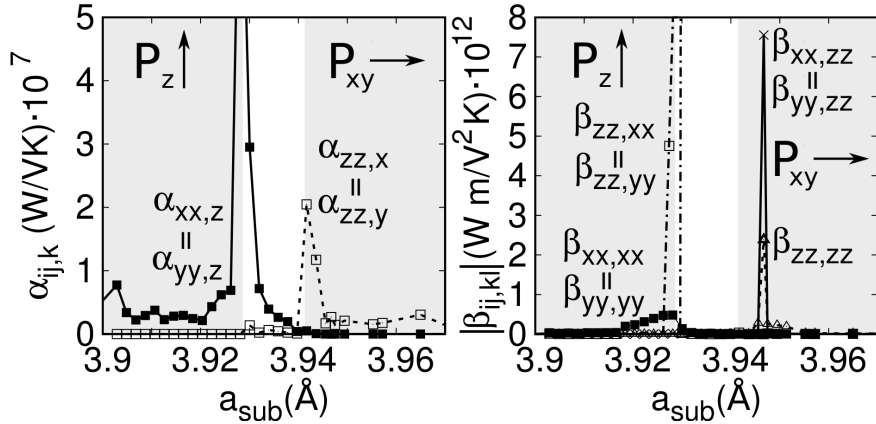


FIG. 4: (Left) First-order electrophononic coefficient,  $\alpha_{ii,j}$ , with  $i \neq j$ , and (right) second-order electrophononic coefficient,  $\beta_{ii,ii}$  and  $\beta_{ii,jj}$ , with  $i \neq j$ , as a function of the substrate lattice parameter  $a_{sub}$ . The polarization direction is represented to indicate when  $\mathbf{E}$  is perpendicular or in the plane of  $\mathbf{P}$ .

strains.

To better characterize the electric field induced reduction of the thermal conductivity and the interplay of the electrophononic response with the epitaxial strain, in Fig. 5 we have represented the percentage reduction of  $\kappa$  as a function of strain at a given electric field. It can be observed that close to the critical strains reductions of the thermal conductivity up to 60% can be easily obtained by applying a small electric field of  $E_i = 5 \times 10^4$  V/cm. Notice that the overall reduction of the thermal conductivity has two components: at first it decreases as a result of an applied strain close to the critical value, then it further decreases when the electric field is applied. These components can be dynamically tuned with high precision by using a piezoelectric substrate for the former and by an external bias for the latter.

In conclusion we have studied the interplay between the biaxial strain and the electrophononic response in a paradigmatic ferroelectric perovskite. We have analyzed the tendency to move from an out-of-plane to an in-plane polarization at a critical tensile strain and shown that this effortless and spontaneous reorientation of the polarization results in giant electrophononic responses, at least one order of magnitude larger than those reported in

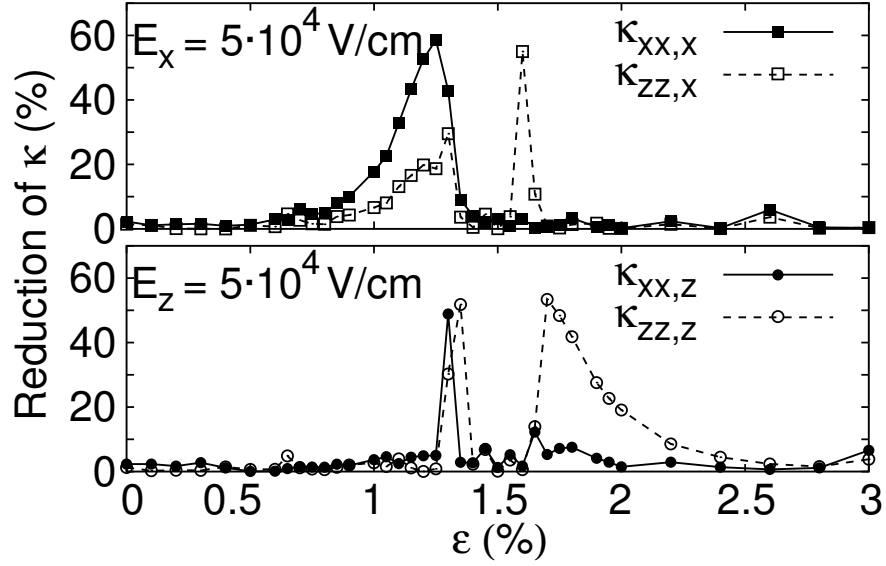


FIG. 5: Reduction of the lattice thermal conductivity as function of strain for electric fields of  $E_i = 5 \times 10^4$  V/cm along the x-axis (top) and the z-axis (bottom). The same electrophononic response for  $\kappa_{xx,x}$  and  $\kappa_{xx,z}$  is found for  $\kappa_{yy,y}$  and  $\kappa_{yy,z}$ .

the unstrained system, thus enabling the manipulation of the phonon flux with vanishingly small electric fields. Since the underlying physical mechanisms are robust and not specific to certain materials or vibrational characteristics, these effects can potentially be exploited in a broader class of materials.

### Acknowledgments

We acknowledge financial support by the Ministerio de Economía, Industria y Competitividad (MINECO) under grants FEDER-MAT2017-90024-P and the Severo Ochoa Centres of Excellence Program under Grant SEV-2015-0496 and by the Generalitat de Catalunya under grant no. 2017 SGR 1506. Work in Luxembourg was funded by the Luxembourg National Research Fund (Grant No. FNR/C18/MS/12705883/REFOX/Gonzalez). We thank the Centro de Supercomputación de Galicia (CESGA) for the use of their computational

resources.

---

- [1] N. Li, J. Ren, L. Wang, G. Zhang, P. Hänggi, and B. Li, *Rev. Mod. Phys.* **84**, 1045 (2012).
- [2] S. Volz, J. Ordonez-Miranda, A. Shchepetov, M. Prunnila, J. Ahopelto, T. Pezeril, G. Vaudel, V. Gusev, P. Ruello, E. M. Weig, et al., *Eur. Phys. J. B* **89**, 15 (2016).
- [3] I. Zardo and R. Rinaldi, *Curr. Opin. Green Sustain. Chem.* **17**, 1 (2019).
- [4] E. Pop, *Nano Research* **3**, 147 (2010).
- [5] G. Benenti, G. Casati, K. Saito, and R. S. Whitney, *Physics Reports* **694**, 1 (2017).
- [6] X. Moya, E. Defay, N. D. Mathur, and S. Hirose, *MRS Bulletin* **43**, 291 (2018).
- [7] M. Terraneo, M. Peyrard, and G. Casati, *Phys. Rev. Lett.* **88**, 094302 (2002).
- [8] B. Li, L. Wang, and G. Casati, *Phys. Rev. Lett.* **93**, 184301 (2004).
- [9] B. Li, L. Wang, and G. Casati, *Appl. Phys. Lett.* **88**, 143501 (2006).
- [10] J. A. Seijas-Bellido, C. Escorihuela-Salayero, M. Royo, M. P. Ljungberg, J. C. Wojdeł, J. Íñiguez, and R. Rinaldi, *Phys. Rev. B* **96**, 140101 (2017).
- [11] M. Royo, C. Escorihuela-Salayero, J. Íñiguez, and R. Rinaldi, *Phys. Rev. Materials* **1**, 051402 (2017).
- [12] J. A. Seijas-Bellido, H. Aramberri, J. Íñiguez, and R. Rinaldi, *Phys. Rev. B* **97**, 184306 (2018).
- [13] P. Torres, J. A. Seijas-Bellido, C. Escorihuela-Sayalero, J. Íñiguez, and R. Rinaldi, *Phys. Rev. Materials* **3**, 044404 (2019).
- [14] J. A. Seijas-Bellido, J. Íñiguez, and R. Rinaldi, submitted (2019).
- [15] D. G. Schlom, L.-Q. Chen, C.-B. Eom, K. M. Rabe, S. K. Streiffer, and J.-M. Triscone, *Annu. Rev. Mater. Res.* **37**, 589 (2007).
- [16] K. Iida, Y. Sugimoto, T. Hatano, T. Urata, M. Langer, B. Holzapfel, J. Hänisch, and H. Ikuta, *Appl. Phys. Express* **12**, 016503 (2019).
- [17] R. K. Zheng, C. Chao, H. L. W. Chan, C. L. Choy, and H. S. Luo, *Phys. Rev. B* **75**, 024110 (2007).
- [18] P. García-Fernández, J. C. Wojdeł, J. Íñiguez, and J. Junquera, *Phys. Rev. B* **93**, 195137

(2016), URL <https://www.secondprinciples.unican.es/>.

- [19] J. C. Wojdeł, P. Hermet, M. P. Ljungberg, P. Ghosez, and J. Íñiguez, *J. Phys.: Condens. Matter* **25**, 305401 (2013).
- [20] P. Zubko, J. C. Wojdeł, M. Hadjimichael, S. Fernandez-Pena, A. Sené, I. Luk'yanchuk, J. Triscone, and J. Íñiguez, *Nature* **534**, 524 (2016).
- [21] P. Shafer, P. García-Fernández, P. Aguado-Puente, A. R. Damodaran, A. K. Yadav, C. T. Nelson, S.-L. Hsu, J. C. Wojdeł, J. Íñiguez, L. W. Martin, et al., *Proc. Natl. Acad. Sci.* (2018).
- [22] A. Togo and I. Tanaka, *Scr. Mater.* **108**, 1 (2015).
- [23] W. Li, N. Mingo, L. Lindsay, D. A. Broido, D. A. Stewart, and N. A. Katcho, *Phys. Rev. B* **85**, 195436 (2012).
- [24] W. Li, J. Carrete, N. A. Katcho, and N. Mingo, *Comp. Phys. Commun.* **185**, 1747 (2014).
- [25] A. Ward, D. A. Broido, D. A. Stewart, and G. Deinzer, *Phys. Rev. B* **80**, 125203 (2009).
- [26] P. Torres, F. X. Alvarez, X. Cartoixà, and R. Rurali, *2D Mater.* **6**, 035002 (2019).
- [27] S. Tamura, *Phys. Rev. B* **27**, 858 (1983).
- [28] O. Diéguez, S. Tinte, A. Antons, C. Bungaro, J. B. Neaton, K. M. Rabe, and D. Vanderbilt, *Phys. Rev. B* **69**, 212101 (2004).
- [29] O. Diéguez, K. M. Rabe, and D. Vanderbilt, *Phys. Rev. B* **72**, 144101 (2005).
- [30] C. Cazorla and M. Stengel, *Phys. Rev. B* **92**, 214108 (2015).
- [31] G. Kresse and J. Furthmüller, *Phys. Rev. B* **54**, 11169 (1996).
- [32] P. E. Blöchl, *Phys. Rev. B* **50**, 17953 (1994).
- [33] G. Kresse and D. Joubert, *Phys. Rev. B* **59**, 1758 (1999).
- [34] M. Tachibana, T. Kolodiaznyi, and E. Takayama-Muromachi, *Appl. Phys. Lett.* **93**, 092902 (2008).
- [35] J. C. Wojdeł and J. Íñiguez, *Phys. Rev. Lett.* **112**, 247603 (2014).
- [36] A. García and D. Vanderbilt, *Appl. Phys. Lett.* **72**, 2981 (1998).